



Article

Conversion of Triaxial Compression Strain–Time Curves from Stepwise Loading to Respective Loading

Haigang Qu ¹, Dianrui Mu ¹, Zhong Nie ² and Aiping Tang ^{1,*}¹ School of Civil Engineering, Harbin Institute of Technology, Harbin 150090, China² Engineering Research Institute of Appraisal and Strengthening of Shandong Jianzhu University Co., Ltd., Jinan 250014, China

* Correspondence: apt_hit@126.com

Abstract: Numerous researchers of soil creep behavior adopt stepwise loading (SL) rather than respective loading (RL) to perform the triaxial creep tests. However, a complete continuous strain–time curve of SL needs to be converted into assumed curve clusters supposing obtained under RL before the deformation data are used to develop creep constitutive models. Classical methods realize the conversion mainly by focusing on the creep deformation parts and classifying them into linear and nonlinear compositions. Mostly, the linear parts are simply superposed while the nonlinear parts are complex to consider and so are neglected. Moreover, classical methods are not sufficiently valid to eliminate the stress history effect on the conversion. Here, a new method is proposed to achieve the conversion without neglecting the stress history effect. The method rebuilds the triaxial creep test mathematically and physically, adhering to the revising of energy. The method treats the tested deformation in its entirety, instead of distinguishing it into elastic, visco-elastic, plastic and creep (linear and nonlinear) deformation to convert respectively. The comparison among actual measured SL and RL strain–time curves and the curves converted by the new method proves the stress history effect should not be neglected. The higher the vertical load level, the larger the discrepancy between the RL and SL strain–time curve, and the disparity becomes larger with time. The new method highlights the necessity of considering the stress history effect in analysis and design for higher accuracy. The comparisons illustrate the conversion method at least produces more satisfactory results for clayey soil. Primarily examined, at the later stages of loading, the disparity in strain between the converted RL and measured RL decreases by 52.5%~53.5% compared with strain between the measured SL and measured RL.

Keywords: soft soil; creep; strain–time curve; stepwise loading; respective loading

Citation: Qu, H.; Mu, D.; Nie, Z.; Tang, A. Conversion of Triaxial Compression Strain–Time Curves from Stepwise Loading to Respective Loading. *Geotechnics* **2022**, *2*, 855–870. <https://doi.org/10.3390/geotechnics2040041>

Academic Editor: Daniel Dias

Received: 10 August 2022

Accepted: 27 September 2022

Published: 30 September 2022

Publisher's Note: MDPI stays neutral with regard to jurisdictional claims in published maps and institutional affiliations.



Copyright: © 2022 by the authors. Licensee MDPI, Basel, Switzerland. This article is an open access article distributed under the terms and conditions of the Creative Commons Attribution (CC BY) license (<https://creativecommons.org/licenses/by/4.0/>).

1. Introduction

Time-dependent stress–strain behavior is a basic research theme of geotechnical engineering. To obtain realistic solutions for time-dependent engineering problems, it is essential to use a constitutive model that accounts for the time dependency of the stress–strain–strength properties of soils. The research on soil creep behavior and properties is a significant branch of soil rheology research. So far, considerable creep constitutive models have been developed from laboratory tests and then adopted in numerical simulation and practical engineering [1]. Therefore, laboratory tests potentially affect the constitutive models.

1.1. Loading Mode

In laboratory triaxial rheological tests, there are two modes to exert the vertical axial stress loads ($\sigma_1 - \sigma_3$): respective loading (RL) and stepwise loading (SL).

SL is exerting a series of loads in turn to only one soil specimen, with each load level sustained until the specimen is deformed extremely slowly towards a relatively steady

state. SL produces the stress–strain–time data from a single specimen that experienced a series of loads.

RL is exerting certain constant axial loads to soil specimens one to one. Tests in this loading mode measure and record the strain–time behavior of soil specimens accurately from an initial unpressed state to its failure or unacceptable deformation state.

Usually, RL is considered closer to the concept of research on soil mechanical behavior over time with constant stress load, while in building engineering, the fact is that the total load is not exerted on the soil at one time but gradually, which is coordinated with SL. Even if soil creep behavior is considered from the moment that a building is put into service, there still exists a stress history effect because the soil withstanding forces from the upper building has already been pressed to be dense. Furthermore, if there are not enough rheometers to carry out several tests simultaneously, RL will be time-consuming [2]. Analyzing the data obtained from RL is affected by soil specimens being discrete in physical properties as well as loading conditions (environmental vibrations, temperature, etc.) being slightly different. Therefore, SL has been chosen for numerous creep research studies of soil and rock for a long time up to now [3–14].

1.2. Strain–Time Curves and Creep Curves

Here, firstly, the ‘strain–time curve’ is distinguished from the ‘creep curve’. The former contains all the total strain–time points recorded from the moment that the stress load reaches the preset value. The ‘strain’ is composed of elastic, visco-elastic, plastic, and creep strain, while only the latter contains the creep strain–time part. Nowadays, whether the effective stress of the soil specimen is stable is used to judge whether the creep deformation has begun. At an early stage, when the effective stress cannot be measured accurately, there was no unified criterion for the judgement of elastoplastic and creep strain, and some scholars adopt one hour from when the load stress became stable as the time demarcation point for the two types of strain [15–17]. There also exist some research works which treat ‘strain–time curve’ as ‘creep curve’ [18], however, here, we do not follow this view.

Though the strain–time curves of SL have practical significance, as mentioned in Section 1.1, researchers prefer the strain–time curves of RL to develop a constitutive model, avoiding the soil stress history effect [19]. Figure 1a shows the single stair-shaped creep curves of RL and Figure 1b shows the multi-stair-shaped creep curves of SL. Though the curves of SL contain the stress history effect of former load levels to latter load levels, researchers began to convert the tested creep deformation curves of SL into assumed curves of RL from an early stage [2,3,20].

The problem is as follows: in the gradually uplifted multi-stair-shaped deformation curve of SL, the latter sections are actually affected by the former sections. There exist micro fissures in the specimen caused by former loads when the latter loads are to be exerted and the fissures exacerbate deformation [21]. How to convert the curves to get rid of the stress history effect remains a problem [2].

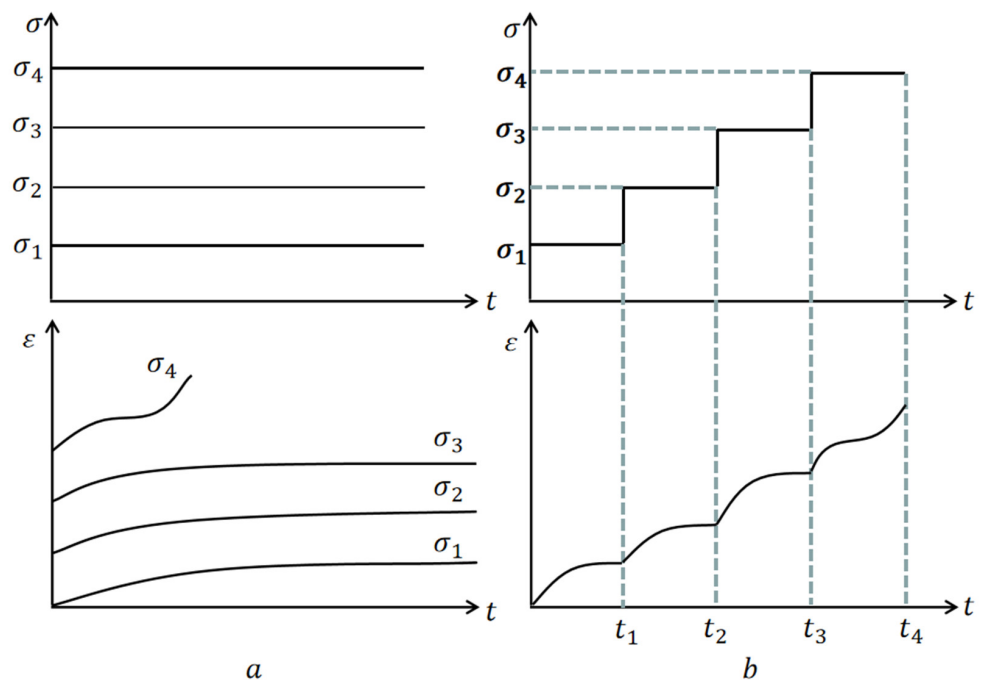


Figure 1. (a): RL mode and corresponding creep strain–time curves. (b): SL mode and corresponding creep strain–time curves [2].

1.3. Classical Conversion Methods for Creep Curves

1.3.1. The Coordinate Translation Method (CTM)

This method was too simple to be first thought of to perform the conversion: each beginning moment of a stair loading is regarded as the initial moment of the creep curve under the corresponding RL level, and the subsequent time is counted from this moment, that is, the time coordinate is dragged backward. This method is based on the Boltzmann linear superposition method [22] for the linearly viscoelastic body of rock. Here, the soil is assumed to be linearly rheological [23]. The linearly rheological property means that though the constitutive relationship ($\sigma - \epsilon$) varies with time, at the same moment, the ($\sigma - \epsilon$) relationship always remains linear [24].

The CTM holds that the total creep deformation of the specimen is the linear superposition of the creep deformation increments caused by each load level, and the deformation effect of each load level on the specimen is independent. However, in most cases, the soil is not linearly rheological and the creep deformation is actually affected by the former load levels. What is more, the linear superposition requires that the time of exerting each load level must be consistent, and the creep deformation rate must be close to zero so that the next load level can be exerted. In most creep tests, the time needed for the creep deformation to be stable increases with the load level, so it is difficult to determine each loading duration in advance.

1.3.2. Chen’s Method (Tan’s Method)

Tjong-kie Tan and Wen-fa Kang [3,20] came up with the experimental skill and drawing method. They tested the torsional creep behavior of sandstone and the mode of multi-stepwise moment loading was

$$M = M_0H(t) + M_1H(t - \theta_1) + M_2H(t - \theta_1) + \dots + M_nH(t - \theta_n) \tag{1}$$

which had been proposed by Tjong-kie Tan earlier in 1964. Towards the multi-stair-shaped creep deformation curve, a geometrical method is used, shown in Figure 2, where b1~b7 are the creep deformation effects caused by the moment increment (921.25 – 612.50) KG-CM and c1~c7 are the creep deformation effects caused by the moment increment

(1254.90 – 921.50) KG-CM. $b_1 \sim b_7$ are considered as the differences between the actual measured creep deformation and the assumed developed creep deformation along $a_1 \sim a_7$ by extending the creep curve under 612.50 KG-CM. The same applies to $c_1 \sim c_7$ under the moment increment (1254.90 – 921.50) KG-CM. Then, the creep curve of RL under 921.25 KG-CM can be obtained by $a_1 + b_1, a_2 + b_2, a_3 + b_3 \dots a_7 + b_7$ and the curve under 1254.90 KG-CM can be drawn by $a_1 + b_1 + c_1, a_2 + b_2 + c_2, a_3 + b_3 + c_3 \dots a_7 + b_7 + c_7$. Chen’s method requires the loading duration of each load level to be the same. Some scholars once explained the theory of this method, also related to the Boltzmann linear superposition method [18]. It has been proved that Chen’s method is better than the CTM [25]. So far, Chen’s method has been considered reasonable for clay hollow tube torsional creep tests and solid cylindrical sandstone torsion tests [20], while valid examination of Chen’s method on triaxial creep tests itself has not been directly found by the authors.

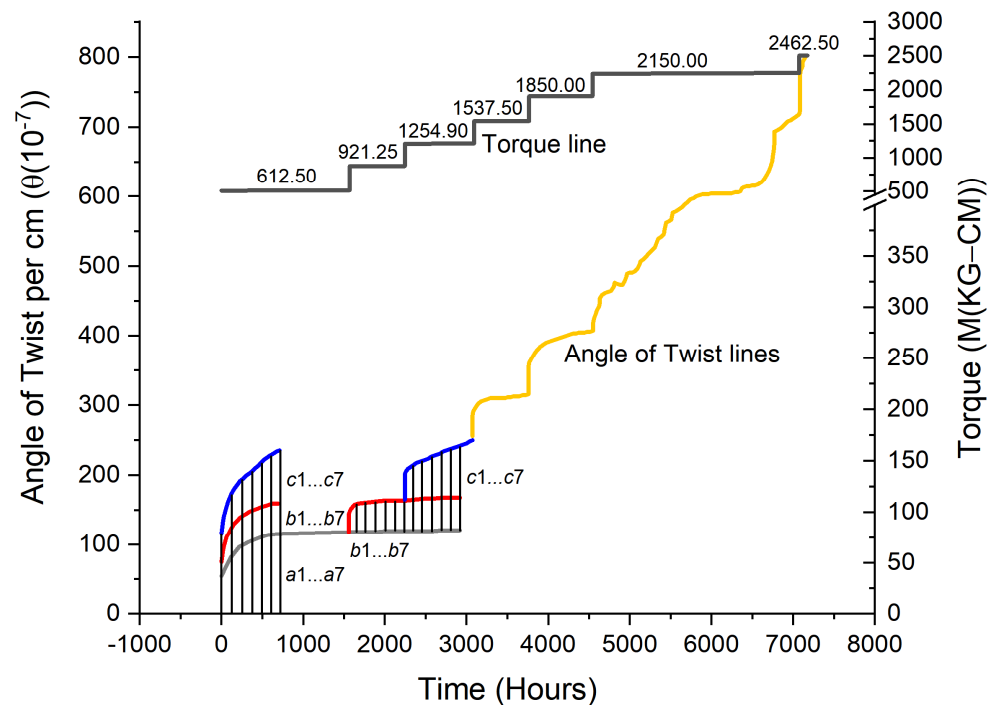


Figure 2. SL creep curve for sandstone and its conversion to RL creep curve [20]. The colors of angle of twist per cm–time lines represent the following: gray line, under 612.50 KG-CM torque; red lines, under 921.25 KG-CM torque; blue lines, under 1254.90 KG-CM torque; yellow line, under other later torque levels.

1.3.3. Sun’s Conversion Method

Jun Sun considers soil to be non-linearly rheological [2]. Suppose the nonlinear creep response is

$$\epsilon_T(t) = \sigma J_1(t) + \sigma^2 J_2(t, t) + \sigma^3 J_3(t, t, t) + \dots \tag{2}$$

where $J_1(t)$ is linear creep compliance of soil, and $J_2(t, t), J_3(t, t, t) \dots$ are a series of nonlinear material functions, all of which are determined by the practical properties and states of the geotechnical materials.

Towards the stress increment $\Delta\sigma_i$ at time t_i , the creep response is

$$\epsilon_i(t) = \Delta\sigma_i J_1(t - t_i) + (\Delta\sigma_i)^2 J_2(t - t_i, t - t_i) + (\Delta\sigma_i)^3 J_3(t - t_i, t - t_i, t - t_i) + \dots \tag{3}$$

Different from the linearly rheological hypothesis, Equation (3) reflects the effects of higher-order stress terms. The total response $\epsilon_T(t)$ at any time t covers both linear and nonlinear effects. The nonlinear effects exist in the contribution of the interactions among the higher-order increments of stress and each stress level.

That is

$$\begin{aligned} \varepsilon_i(t) = & \Delta\sigma_0 J_1(t) + \Delta\sigma_1 J_1(t - t_1) + \Delta\sigma_2 J_1(t - t_2) + \dots + (\Delta\sigma_1)^2 J_2(t, t) + \Delta\sigma_0 J_2(t, t - t_1) + \Delta\sigma_1 \Delta\sigma_0 J_2(t - t_1, t) \\ & + (\Delta\sigma_1)^2 J_2(t - t_1, t - t_1) + \Delta\sigma_0 \Delta\sigma_2 J_2(t, t - t_2) + \dots + (\Delta\sigma_0)^3 J_3(t, t, t) + (\Delta\sigma_0)^2 \Delta\sigma_1 J_3(t, t, t - t_1) + \dots \\ & + \Delta\sigma_0 \Delta\sigma_1 \Delta\sigma_2 J_3(t, t - t_1, t - t_2) + \dots \end{aligned} \tag{4}$$

Therefore, the total strain under multi-load levels can be expressed as:

$$\varepsilon_T(t) = \sum \Delta\sigma_i J_1(t - t_i) + \sum \sum \Delta\sigma_i \Delta\sigma_j J_2(t - t_i, t - t_j) + \sum \sum \sum \Delta\sigma_i \Delta\sigma_j \Delta\sigma_k (t - t_i, t - t_j, t - t_k) + \dots \tag{5}$$

If stress changes continuously with time, the sum form of Equation (5) will become the integrated form. When $J_2, J_3 \dots$ is omitted, Equation (5) becomes the Boltzmann linear superposition method. Although Equation (5) is presented in an analytic form, it is difficult for practical application, because the nonlinear material functions $J_2(t, t), J_3(t, t, t) \dots$ must be determined by additional experiments.

Comparing the CTM, Chen’s method, and Sun’s conversion method, the former two methods cannot effectively consider the non-linearity of strain–time properties and eliminate the stress history effect, while Sun’s method requires extra tests which consume more time and effort. In this manuscript, the loading mode effect on the triaxial compression strain–time curves is discussed and attempts are made to eliminate it, so that the creep constitutive model of higher accuracy can be proposed and calibrated based on the curves.

2. Method—The Revise Energy Method (REM) for the Conversion of the Strain–Time Curves

As introduced in Section 1.3, the classical methods for the conversion mainly focus on creep strain–time. This is because the researchers only needed the creep strain parts at that time, and the conversion mainly starts from the perspective of ‘strain’, not ‘deformation’. These methods are based on the concept of classifying strain as linear and nonlinear.

The REM will perform the conversion on deformation, treating deformation as an entirety, to obtain the RL strain–time curves corresponding to SL.

Take the example of exerting the first two load levels in turn (SL) and exerting equal loads at one time (RL). Figure 3a shows the process of exerting the first stepwise load F_1 and Figure 3b shows that of adding the second SL F_2 on the same specimen A. Figure 3c shows the RL of the same load F_1 on specimen B. Figure 3d shows the RL of the same load $F_1 + F_2$ on specimen C.

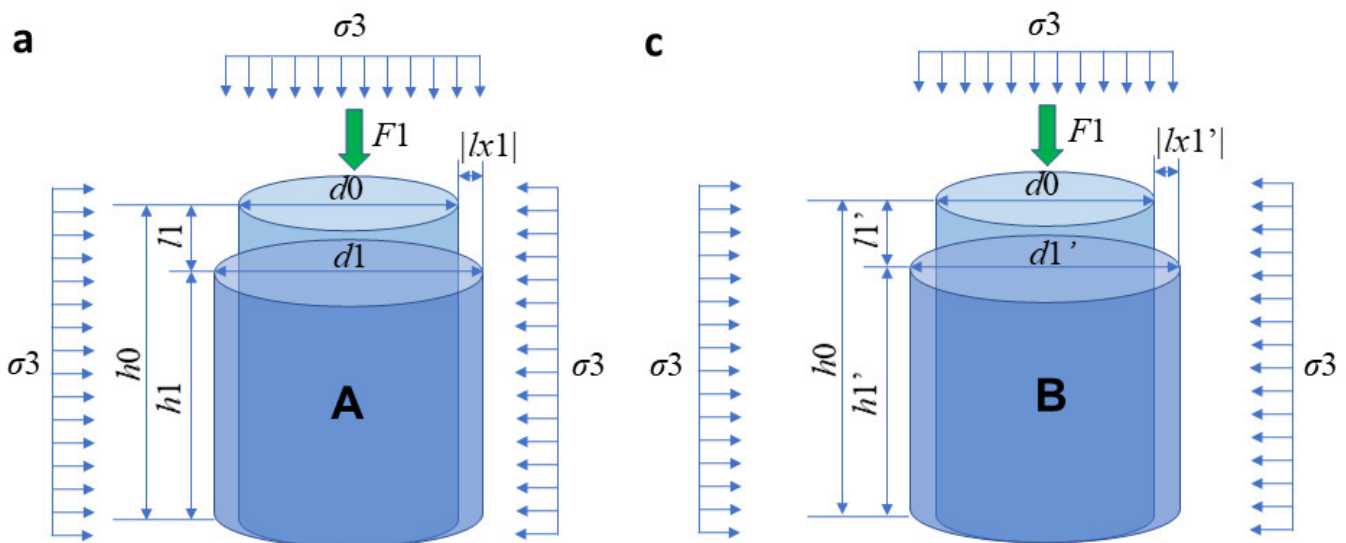


Figure 3. Cont.

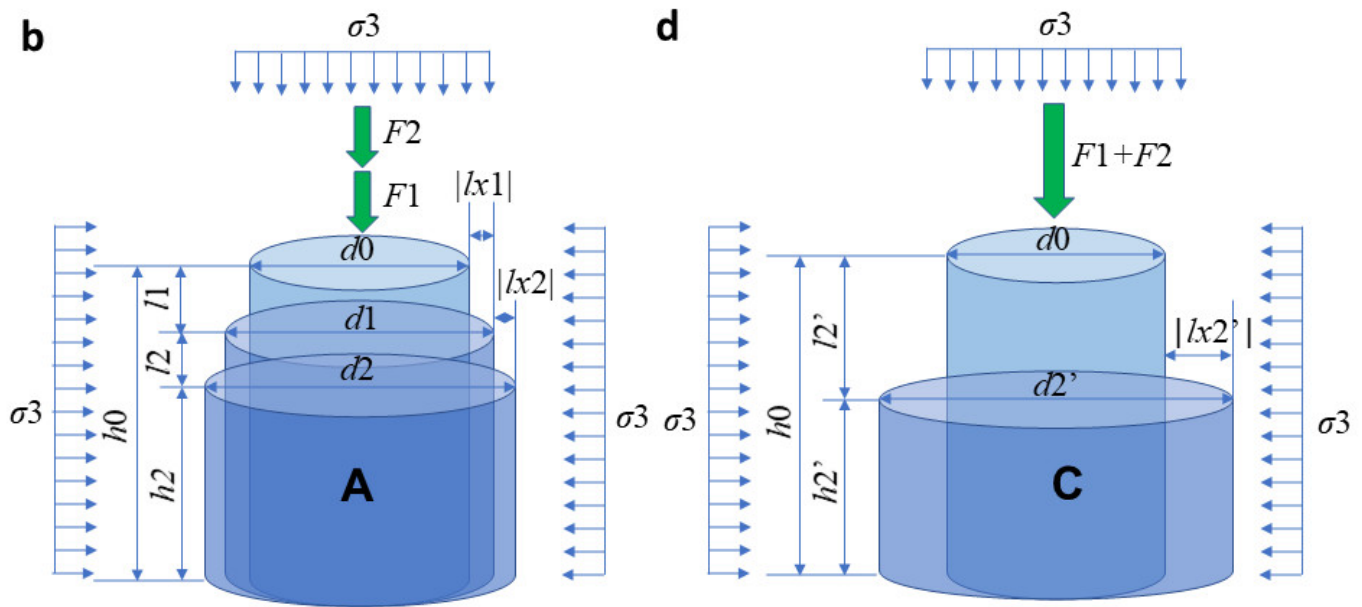


Figure 3. Illustration of SL process on specimen A and RL process on specimen B and C. (a) Specimen A is deformed under F_1 load. (b) Specimen A is continually deformed under another F_2 load after it reached a stable deformation state under F_1 load. (c) Specimen B is deformed under F_1 load. (d) Specimen C is deformed under $(F_1 + F_2)$ load.

The SL and RL of F_1 will result in the same deformation. The actual deformation conversion should begin from the $+F_2$ loading on specimen A and $F_1 + F_2$ loading on specimen C.

Conservation of energy is usually used as a process calculation criterion from the beginning to the end. When the specimen is deformed to the stable state under the 2nd level SL, the external force work W_2 should be expressed as

$$W_2 = F_1(l_1 + l_2) + F_2l_2 + \int_{t_0}^{t_1} \int_0^{l_1} (\sigma_3 \cdot A_t) dl dt + \int_{t_1}^{t_2} \int_0^{l_2} (\sigma_3 \cdot A_t) dl dt + \int_{t_0}^{t_1} \int_0^{l_{x1}} (\sigma_3 \cdot A_s) dl_x dt + \int_{t_1}^{t_2} \int_0^{l_{x2}} (\sigma_3 \cdot A_s) dl_x dt \quad (6)$$

To simplify the explanation of so many symbols in the manuscript, here, we extend the constant subscripts to variable subscripts and explain them. The symbols with superscripts represent similar meanings while under RL, if not explained specially.

W_n is the total external force work of n vertical load levels under SL.

n is the level of vertical SL at present or to be calculated.

F_i is the i th external vertical load. It is the single load under SL, not the accumulated loads, (N). $i = 1, \dots, n$.

$l_j (l_{xj})$ is the vertical stable deformation increment (the mean radial swell increment) under the j th SL compared with the $(j - 1)$ th loading, (mm). $j = 1, \dots, n$.

σ_3 is the confining pressure under SL, (MPa). (σ'_3 , under RL).

$A_t (A_s)$ is the top (side) area of the triaxial specimen under SL, (mm²). (A'_t , under RL) (A'_s , under RL).

t_{i-1}, t_i are, respectively, the beginning time and the stable time of the i th SL, (min). $t_0 = 0$.

$A_s, A_t, \sigma_3 (A'_s, A'_t, \sigma'_3)$ change with time.

By setting the value adoption mode of the physical terms in the integral Equation (6), Equation (6) can be simplified as

$$W_2 = F_1(l_1 + l_2) + F_2l_2 + \sigma_3 \cdot A_{t1} \cdot l_1 + \sigma_3 \cdot A_{t2} \cdot l_2 + \sigma_3 \cdot A_{s1} \cdot l_{x1} + \sigma_3 \cdot A_{s2} \cdot l_{x2} \quad (7)$$

A_{ti} (A_{si}) is the stable top (side) area of the triaxial specimen under the i th level SL, (mm^2). (A'_{ti} , under RL F'_i) (A'_{si} , under RL F'_i) (Note: the load at this moment is accumulated loads of all the former load levels).

(Note: σ_3 is actually changeable during the test process, but few experiments performed earlier chose to change it because a complex stress history will make the analysis more difficult.)

When the equal level RL test develops to the steady state, the external force work W'_2 should be expressed as

$$W'_2 = F'_2 l'_2 + \int_{t_0}^{t'_2} \int_0^{l'_2} (\sigma'_3 \cdot A'_t) dl' dt + \int_{t_0}^{t'_2} \int_0^{l'_{x2}} (\sigma'_3 \cdot A'_s) dl'_{x2} dt \tag{8}$$

where W'_n is the total external force work of n vertical load levels under RL.

n is the level of vertical RL at present or needs to be calculated. For RL, $i = n$.

F'_i is the i th external vertical load. It is the single load under RL, equaling the total quantity from 1st to i th load level under SL, (N). The same, $i = n$ for RL.

l'_i is the vertical stable deformation under the F'_i RL, (mm).

l'_{xi} is the mean radial swell increment under the F'_i RL, (mm).

t'_i is the time needed until the stable deformation under the F'_i RL, (mm). $t_0 = 0$.

Usually, the conversion of strain–time (deformation–time) curves from SL to RL keeps the confining pressure the same: $\sigma_3 = \sigma'_3$.

Similarly to Equation (7), Equation (8) can be simplified as below

$$W'_2 = F'_2 l'_2 + \sigma_3 \cdot A'_{t2} \cdot l'_2 + \sigma_3 \cdot A'_{s2} \cdot l'_{x2} \tag{9}$$

The conversion process of strain–time (deformation–time) curves is to convert the known practical deformation under SL to the unknown deformation under RL. The connection, that is, the consistency equation, could be keeping the total external force work of the i th load level the same between two loading modes:

$$W_2 = W'_2 \tag{10}$$

However, by comparing Equations (7) and (9), there apparently exists a disparity in external force work. With further research, the revised energy term ΔW_2 should be added to W_2 :

$$\Delta W_2 = 2F_2 l_1 + 2[(F_1 + F_2)|\theta| + \sigma_3 \cdot A_{t2} \cdot |\theta|] \tag{11}$$

where θ is a disparity deformation to revise the stress history effect on soil.

$$\theta = \frac{l_1}{F_1} (F_1 + F_2) - (l_1 + l_2) \tag{12}$$

Then Equation (10) is changed into

$$W_2 + \Delta W_2 = W'_2 \tag{13}$$

To obtain the l'_i , Equation (13) is extended by substituting Equations (7), (9) and (11) in, and l'_i should be the only unknown variable. The strain–time (deformation–time) under SL is already known. Clearly, all the other uncertain geometrical variables must be transformed into expressions of the known variables such as l or the unknown variable l'_i , so that Equation (13) can be used to derive the l'_i . The l_{xj} and other geometrical variables may be measured directly if the rheometer is advanced enough [26], which will be considered to be known, making Equation (13) easier.

If the geometrical variables cannot be obtained directly, a hypothesis regarding the geometrical change of the triaxial specimen will push the calculation forward: the triaxial specimen stays in a cylinder shape when it is deformed. This hypothesis refers to the true shape change of specimens in the creep tests, as Figure 4 shows. If there is no friction

between the filter paper and the specimen, and also no friction between the filter paper and the porous stone, the cylinder specimen will keep its cylinder shape [27,28]. Of course, the friction is impossible to avoid, but the l_{xj} , l'_{xi} are both mean values of the radial swell increments, which makes the cylinder hypothesis as approximate as the practical drum-like shape specimen. For UU creep tests, the volume of the cylinder specimen can be assumed not to change, while for the CU and CD, the shrinkage volume of the specimen must be known for higher accuracy.

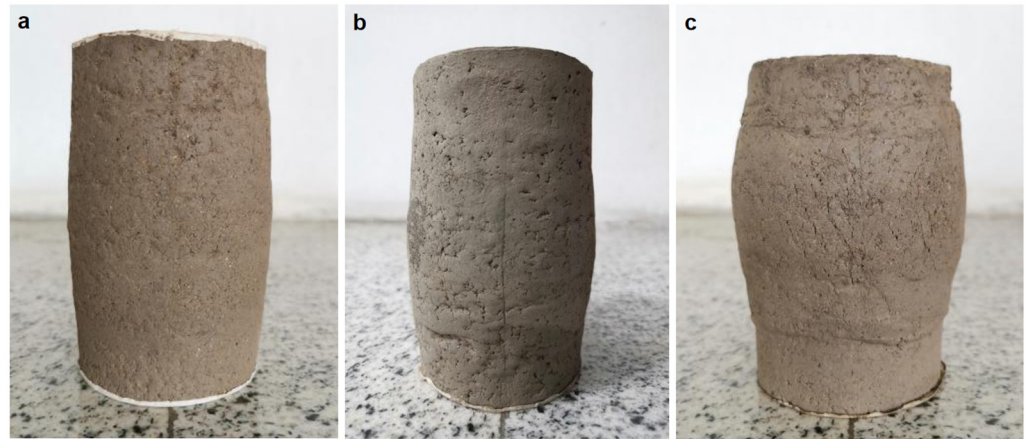


Figure 4. Soil specimen instances after creep tests. Specimen (a), under presupposed confining pressure $\sigma_3 = 200$ kPa. Specimen (b), under presupposed confining pressure $\sigma_3 = 150$ kPa. Specimen (c), under presupposed confining pressure $\sigma_3 = 100$ kPa. $(\sigma_1 - \sigma_3)$ exerted to the three specimens ranges from 37.98 kPa~360.23 kPa. The original sizes of all the three specimens are $d_0 = 61.8$ mm and $h_0 = 125$ mm.

Following the geometrical hypothesis, rebuild the geometrical change of specimens. Take CD creep tests as an example.

For the 1st level SL, the geometrical Equations (14)–(17) are established

$$(1 - \varepsilon_{v1}) \frac{\pi}{4} d_0^2 h_0 = \frac{\pi}{4} d_1^2 h_1 = \frac{\pi}{4} d_1^2 (h_0 - l_1) \tag{14}$$

$$l_{x1} = d_1 - d_0 \tag{15}$$

$$A_{s1} = \pi d_1 h_1 = \pi d_1 (h_0 - l_1) \tag{16}$$

$$A_{t1} = \frac{\pi}{4} d_1^2 \tag{17}$$

While for the same quantity 1st level RL,

$$(1 - \varepsilon'_{v1}) \frac{\pi}{4} d_0^2 h_0 = \frac{\pi}{4} d'_1 h'_1 = \frac{\pi}{4} d'^2_1 (h_0 - l'_1) \tag{18}$$

$$l'_{x1} = d'_1 - d_0 \tag{19}$$

$$A'_{s1} = \pi d'_1 h'_1 = \pi d'_1 (h_0 - l'_1) \tag{20}$$

$$A'_{t1} = \frac{\pi}{4} d'^2_1 \tag{21}$$

where d_0 (h_0) is the initial diameter (height) of the specimen, d_i (h_i) is the stable diameter (height) of the specimen under the i th SL. ε_{vi} is the stable bulk strain of the i th SL. ε'_{vi} is the stable bulk strain of the i th RL.

Similarly, the geometrical equations of the 2nd level SL and the same quantity of the 2nd level RL can be obtained.

$$\text{Obviously, } l'_1 = l_1, l'_{x1} = l_{x1} = d_0 \left(\sqrt{\frac{(1 - \varepsilon'_{v1}) h_0}{h_0 - l'_1}} - 1 \right) = d_0 \left(\sqrt{\frac{(1 - \varepsilon_{v1}) h_0}{h_0 - l_1}} - 1 \right).$$

To obtain l'_2 , a further calculation is needed.

Combine Equations (7), (9), (11)–(13), and the geometrical equations of 2nd level SL and RL. Let $F'_2 = (F_1 + F_2)$, and Equation (22) will be established

$$\begin{aligned} W_2 + \Delta W_2 &= (F_1 + F_2)l'_2 + \sigma_3 A'_{i2} l'_2 + \sigma_3 A'_{s2} l'_{x2} = (F_1 + F_2)l'_2 + \sigma_3 \cdot \frac{\pi}{4} d'^2_2 l'_2 + \sigma_3 \cdot \pi d'_2 h'_2 l'_{x2} \\ &= (F_1 + F_2)l'_2 + \sigma_3 \cdot \frac{\pi}{4} d'^2_2 l'_2 + \sigma_3 \cdot \pi d'_2 (h_0 - l'_2)(d'_2 - d_0) \\ &= (F_1 + F_2)l'_2 + \sigma_3 \cdot \frac{\pi}{4} d_0^2 \left(\frac{(1 - \epsilon'_{v2})h_0}{h_0 - l'_2} \right) l'_2 + \sigma_3 \\ &\quad \cdot \pi d_0 \sqrt{\frac{(1 - \epsilon'_{v2})h_0}{h_0 - l'_2}} (h_0 - l'_2) \left(d_0 \sqrt{\frac{(1 - \epsilon'_{v2})h_0}{h_0 - l'_2}} - d_0 \right) \end{aligned} \tag{22}$$

To simplify Equation (22), let $\sqrt{\frac{(1 - \epsilon'_{v2})h_0}{h_0 - l'_2}} = \xi$, then $l'_2 = \frac{(\xi^2 - 1 + \epsilon'_{v2})}{\xi^2} h_0$, and substitute them back into Equation (22), finally, Equation (23) is

$$\begin{aligned} \frac{1}{4} \pi \sigma_3 d_0^2 h_0 \xi^4 + [(F_1 + F_2)h_0 + \frac{3}{4} \pi \sigma_3 d_0^2 h_0 - \frac{3}{4} \pi \epsilon'_{v2} \sigma_3 d_0^2 h_0 - (W_2 + \Delta W_2)] \xi^2 - (\sigma_3 \pi d_0^2 h_0 - \epsilon'_{v2} \pi \sigma_3 d_0^2 h_0) \xi \\ + (F_1 + F_2)(\epsilon'_{v2} - 1)h_0 = 0 \end{aligned} \tag{23}$$

To solve l'_2 , ξ should be solved first. Fortunately, Equation (23) is a quartic equation of one variable, which is solvable analytically. However, unless the RL is practically performed, ϵ'_{v2} will not be determined, so ϵ_{v2} which can be measured in SL is used instead. It should also be noted,

$$\begin{aligned} (1 - \epsilon'_{vi}) \frac{\pi}{4} d_0^2 h_0 = \frac{\pi}{4} d'^2_i h'_i = \frac{\pi}{4} d'^2_i (h_0 - l'_i) \rightarrow d'_i = d_0 \sqrt{\frac{(1 - \epsilon'_{vi})h_0}{h_0 - l'_i}} \rightarrow \nu = \left(\frac{d_0 - d'_i}{d_0} \right) / \left(\frac{l'_i}{h_0} \right) \\ = \left(\frac{d_0 - d_0 \sqrt{\frac{(1 - \epsilon'_{vi})h_0}{h_0 - l'_i}}}{d_0} \right) / \left(\frac{l'_i}{h_0} \right) = \frac{h_0}{l'_i} \left(1 - \sqrt{\frac{(1 - \epsilon'_{vi})h_0}{h_0 - l'_i}} \right) \end{aligned} \tag{24}$$

Here, ν is the Poisson ratio of the triaxial cylinder specimen at the stable state. With the proper time interval selected, the real-time Poisson ratio will also be obtained in the same way.

On working out the ξ , l'_2 is also obtained.

Repeat the calculation idea and steps until the n th loading, and Equation (23) will be extended as

$$\begin{aligned} \frac{1}{4} \pi \sigma_3 d_0^2 h_0 \xi^4 + \left[\left(\sum_{i=1}^n F_i \right) h_0 + \frac{3}{4} \pi \sigma_3 d_0^2 h_0 - \frac{3}{4} \pi \epsilon_{vn} \sigma_3 d_0^2 h_0 - (W_n + \Delta W_n) \right] \xi^2 - (\sigma_3 \pi d_0^2 h_0 - \epsilon_{vn} \pi \sigma_3 d_0^2 h_0) \xi \\ + \left(\sum_{i=1}^n F_i \right) h_0 (\epsilon_{vn} - 1) = 0 \end{aligned} \tag{25}$$

$$\xi = \sqrt{\frac{(1 - \epsilon_{vi})h_0}{h_0 - l'_i}} \tag{26}$$

$$l'_i = \frac{(\xi^2 - 1 + \epsilon_{vi})}{\xi^2} h_0 \tag{27}$$

$$\Delta W_n = 2 \sum_{i=2}^n (F_i l_{i-1}) + 2 \left[\left(F_1 + \sum_{i=2}^n F_i \right) |\theta| + \sigma_3 \cdot A_{tn} \cdot |\theta| \right] \tag{28}$$

$$\theta = \frac{l_1}{F_1} \left(F_1 + \sum_{i=2}^n F_i \right) - \left(l_1 + \sum_{i=2}^n l_i \right) \tag{29}$$

In solving Equation (23) or (25), there will be four solutions. According to Equation (27), the useful solution ξ is the positive real number which is slightly more than 1.0.

By now, all the calculation steps in the REM have only finished the conversion of stable deformation points of the deformation–time curves while other points at any time between loading moment and a stable state were not converted. To obtain the complete converted strain–time (deformation–time) curves, the method should be used for the whole process of SL on a specimen.

To reduce the considerable calculation amount, for each stair of a deformation–time curve, select a series of calculation points in a kind of time mode, for example, $t_k = 100k, k = 0, 1, 2, 3 \dots$ (min) as the temporary stable time points until the real end moment of a stair. Carry out the method again by replacing the integral end time point with t_k .

Then there will be a series of quartic equations of ζ

$$\frac{1}{4}\pi\sigma_3 d_0^2 h_0 \zeta_{t_k}^4 + \left[\left(\sum_{i=1}^n F_i \right) h_0 + \frac{3}{4}\pi\sigma_3 d_0^2 h_0 - \frac{3}{4}\pi\varepsilon_{vn,t_k} \sigma_3 d_0^2 h_0 - (W_{n,t_k} + \Delta W_n) \right] \zeta_{t_k}^2 - (\sigma_3 \pi d_0^2 h_0 - \varepsilon_{vn,t_k} \pi \sigma_3 d_0^2 h_0) \zeta_{t_k} + \left(\sum_{i=1}^n F_i \right) (\varepsilon_{vn,t_k} - 1) h_0 = 0 \tag{30}$$

$$\zeta_{t_k} = \sqrt{\frac{h_0(1 - \varepsilon_{vi,t_k})}{h_0 - l'_{t_k}}}, l'_{t_k} = \frac{(\zeta_{t_k}^2 - 1 + \varepsilon_{vi,t_k})}{\zeta_{t_k}^2} h_0 \tag{31}$$

where W_{n,t_k} is the total external force work up to the moment of t_k at n th stair of a deformation–time curve, ($n = 1, 2, 3, \dots, t_k = 100k, k = 1, 2, 3 \dots$). The simplified W_{n,t_k} is

$$W_{n,t_k} = \sum_{i=1}^{n-1} \left(F_i \cdot \sum_{j=i}^{n-1} l_j \right) + F_n \cdot l_{t_k} + \sum_{i=j=1}^{n-1} (\sigma_3 \cdot A_{ti} \cdot l_j) + \sigma_3 \cdot A_{tt_k} \cdot l_{t_k} + \sum_{i=j=1}^{n-1} (\sigma_3 \cdot A_{si} \cdot l_{xj}) + \sigma_3 \cdot A_{st_k} \cdot l_{xt_k} \tag{32}$$

where l_{t_k} (l_{xt_k}) is up to the t_k moment, the vertical deformation increment (the mean radial swell increment) under the SL of $\sum_{i=1}^n F_i$ level, (mm).

A_{tt_k} (A_{st_k}) is up to the t_k moment, the top (side) area of the triaxial specimen under SL of $\sum_{i=1}^n F_i$ level, (mm²).

l'_{t_k} is the vertical deformation up to the t_k moment under the F'_i RL converted from SL, (mm). l'_{t_k} is also the variable that the REM concerns.

ε_{vn,t_k} (ε_{vi,t_k}) is up to the t_k moment, the bulk strain of the specimen under n th (i th) SL.

Perform the conversion at t_k moments, respectively. With the points converted, a complete deformation–time curve of RL can be drawn.

3. Experiment and Result—An Instance for the Revise Energy Method

3.1. Experiment

Here, to examine the validity of the revise energy method, Zhou’s [29] triaxial creep experimental results of the remolded saturated clayey soil are adopted. The basic physical properties are listed in Table 1.

Table 1. Basic physical properties of clayey soil.

Source of Soil	Sampling Depth (m)	Specific Gravity G_s	Moisture Content ω (%)	Void Ratio e_0	Water Limit w_L (%)	Plastic Limit w_P (%)	Density ρ (g/cm ³)	Particle Gradation (mm)		
								>0.075	0.05–0.075	<0.05
West Lake, Hangzhou, China	15–25	2.74	28	0.87	39.2	22	1.872	2.69	3.21	94.1

Through triaxial CU tests, the cohesion of the remolded clayey soil is 2.37 kPa, and the internal friction angle is 16.86°. The triaxial creep test plan was designed as Table 2.

Apparently, Test 4 and 5 are in a stepwise loading path while Test 1, 2, and 3 are in their respective loading path. The specimens tested are all 61.8 mm (d_0) × 125 mm (h_0). The stable criteria for deformation is < 0.01 mm/d. Axial strain–time and bulk strain–time data are both extracted for conversion.

Table 2. Triaxial creep test plan.

Test	Confining Pressure σ_3 (kPa)	Shearing Strength $(\sigma_1 - \sigma_3)_f$ (kPa)	Loading Path $(\sigma_1 - \sigma_3)$
1	400	330	60
2	400	330	120
3	400	330	240
4	400	330	60 → 120 → 180 → 240
5	400	330	120 → 240

3.2. Result

The conversion axial strain–time curves of $(\sigma_1 - \sigma_3) = 120$ kPa & 240 kPa in Test 4 are illustrated in Figures 5 and 6, respectively, and they are also compared with Test 2 and Test 3. While Figure 7 compares the conversion of $(\sigma_1 - \sigma_3) = 240$ kPa in Test 5 and the respective loading result of Test 3. All the conversions are performed with bulk strain tested in stepwise loading because the conversion itself is based on not knowing the bulk strain of the respective loading.

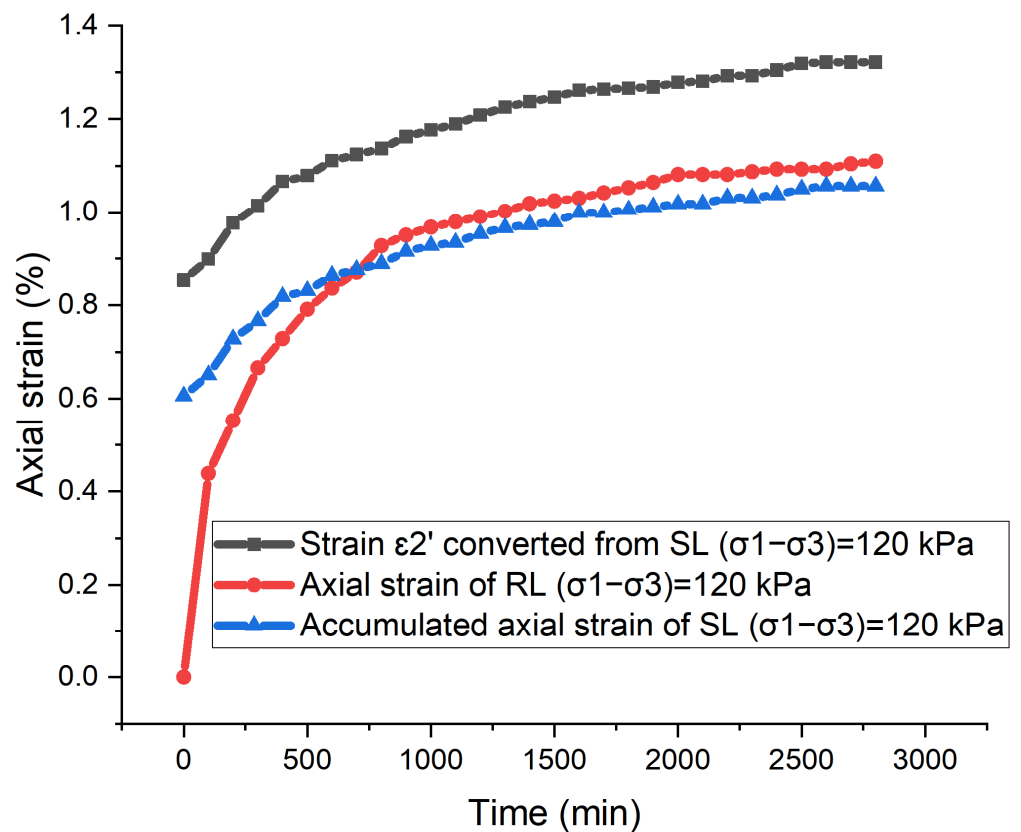


Figure 5. Comparison of converted RL axial deformation and tested RL and SL axial deformation when $(\sigma_1 - \sigma_3) = 120$ kPa (Test 4, 2).

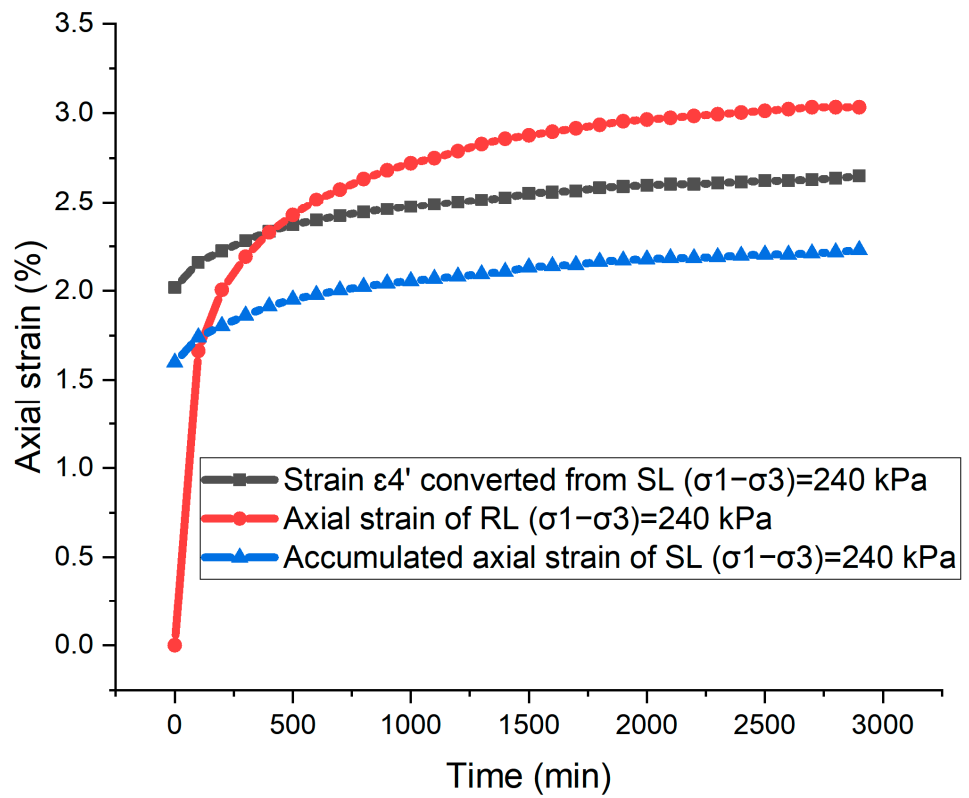


Figure 6. Comparison of converted RL axial deformation and tested RL and SL axial deformation when $(\sigma_1 - \sigma_3) = 240$ kPa (Test 4, 3).

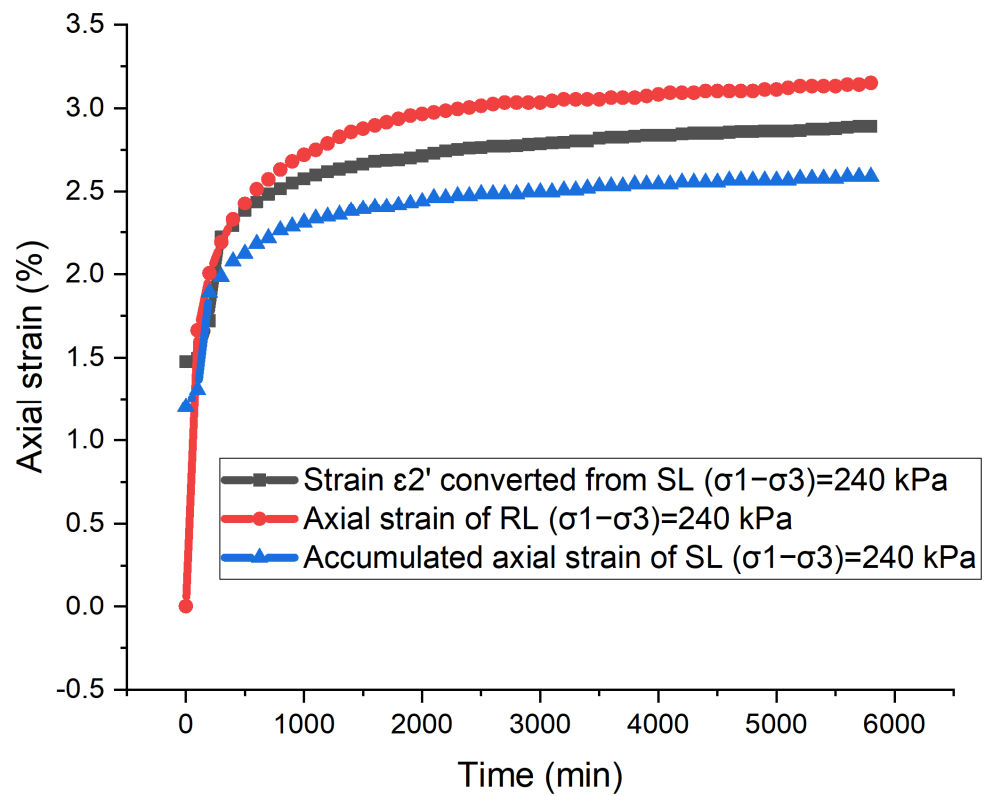


Figure 7. Comparison of converted RL axial deformation and tested RL and SL axial deformation when $(\sigma_1 - \sigma_3) = 240$ kPa (Test 5, 3).

In Figure 5, soil specimens exerted the same external stress load 120 kPa, the SL strain–time curve firstly exceeds the RL curve, while, along with time, the RL curve exceeds the SL curve. The converted strain ϵ'_2 –time (corresponding to l'_2 –time) curve exhibits a higher level than both strain–time of SL and RL. Focusing on the trend that curves develop, in general, the later stage disparity between the converted curve and RL curve becomes smaller, while the disparity between the RL and SL curves becomes larger.

In Figure 6, soil specimens exerted the same external stress load 240 kPa, the RL strain–time curve quickly exceeds the SL curve and later exceeds the converted curve. The converted strain ϵ'_4 –time (corresponding to l'_4 –time) curve exhibits a middle level between the strain–time curves of SL and RL. Focusing on the trend that curves develop, the later stage disparity among the three curves shows an inconspicuous change.

In Figure 7, under the same external stress load of 240 kPa, the RL strain–time curve quickly exceeds the SL curve and the converted curve at an early moment. The converted strain ϵ'_2 –time (corresponding to l'_2 –time) curve exhibits a middle level between the strain–time curves of SL and RL. The later stage disparity among the three curves also shows an inconspicuous change.

4. Discussions—Analysis of the Revise Energy Method

4.1. The Trend Analysis

Usually, within the comparisons of the curves, the RL curve shows a dramatic increase, this is because the RL curve begins from 0 strain at 0 min, while the SL curve, unless it is the first stair, will always begin from a non-zero value in the actual tests and so too the converted curve. In some ways, the differences in beginning points among the curves are the embodiment of the stress history effect. The slope of the RL curve at the beginning stage is greater than the RL and converted curves, corresponding to the elastic modulus variation of the soil specimens. The RL curve is obtained from a specimen in an originally non-loaded state, while the SL curve is obtained from a specimen in an already loaded state, which signifies the latter specimen possesses greater density and higher rigidity (the soil tested is strain-hardening type), and this is also the explanation of stress history effect on the material. It firmly proves again that if the SL curve is adopted for analysis or utilized without conversion, an unsatisfying discrepancy will occur.

The non-zero beginning point cannot be avoided in the conversion because the conversion should be based on already obtained results. To change this, it could be achieved by manually revising the first point of the curve to be (0,0).

At the later stage, with enough loading duration, the specimens are deformed towards a stable state, so the developing tendency of the curves is roughly similar. The tendency of the curves in Figure 5 illustrates the specimens may not have crept to become sufficiently stable.

4.2. The Disparity Analysis

Select the endpoints of all the curves to compare, the strain values are listed in Table 3.

Table 3. End strain of SL, RL, converted strain–time curve of three loading conditions.

Figure (Loading Condition)	End Strain (%)			Disparity of Strain between RL and Converted (%)	Disparity of Strain between RL and SL (%)
	SL Curve	RL Curve	Converted Curve		
1 (120 kPa of Test 2 and 4)	1.06	1.11	1.32	0.21	−0.05
2 (240 kPa of Test 3 and 4)	2.23	3.03	2.65	−0.38	−0.80
3 (240 kPa of Test 3 and 5)	2.59	3.15	2.89	−0.26	−0.56

From the comparison in Table 3, the end strain of the SL curve is generally smaller than it of the RL curve when the loading condition is the same. Comparing the different

loading conditions, the larger the axial stress load is, the larger the discrepancy between the RL and SL strain–time curve is, and the disparity becomes larger with time.

As shown in Figure 8, the strain corresponding to stress $(\sigma_1 - \sigma_3) = 240$ kPa but loaded in different modes also varies. From these tests, in general, the more steps a specimen experiences, the lower the strain level is. These results can both be explained by the stress history effect and the strain hardening property of clayey soil.

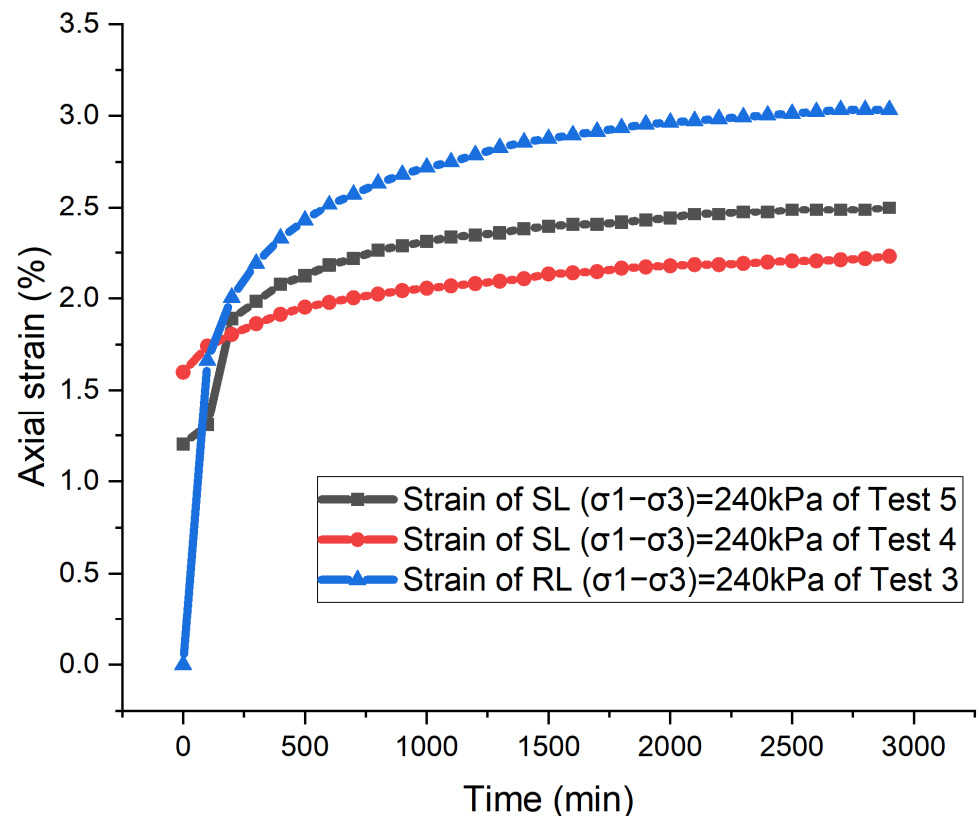


Figure 8. Comparison of axial strain tested in different loading modes when $(\sigma_1 - \sigma_3) = 240$ kPa (Test 3, 4, 5).

As listed in Table 3, the disparity between the actual RL strain and converted strain reaches 0.38% strain. While the disparity between the actual RL and SL reaches 0.8% strain. Therefore, the revise energy method at least improves the accuracy of conversion results at the later stage of deformation with time. Compared with the original SL curves, the converted curves validly approaches the actual RL curves when the stress load becomes larger, while the remaining disparity that the REM is not able to improve may be explained by the fact that:

- 1 The cylinder geometrical hypothesis is not totally applicable to the test results of specimens in shape, as in Figure 4.
- 2 The bulk strain data used in the conversion is tested in SL, not the bulk strain tested in RL, the disparity caused by the discrepancy of bulk strain may be accumulated with the stress load increasing.
- 3 The initial size of the specimen may not accurately be d_0 61.8 mm \times h_0 125 mm, which will not influence the RL strain–time curve decisively but will influence the conversion of REM because d_0 and h_0 are vital parameters for the REM.

The gravity of a triaxial specimen can be neglected in the calculation, however, the gravity of soil cannot be neglected when such a vast amount of soil is involved in the calculation, and the friction must not be neglected either. The practical effect of gravity and friction on the conversion for a large soil test remains for further study.

5. Conclusions

The comparison between actual measured SL and RL strain–time curves proves the stress history effect should not be neglected and highlights the necessity of considering the stress history effect in analysis and design for higher accuracy. For stress hardening soil, the higher the vertical load level is, the larger the discrepancy between the RL and SL strain–time curve is, and the disparity becomes larger with time. In general, to reach a certain stress level, the more steps a specimen experiences, the lower the strain level is.

Through revising the energy relations, the revise energy method rebuilds the triaxial creep test mathematically and physically, eventually achieving the conversion of strain–time curves without neglecting the stress history effect. The method treats the tested deformation as an entirety, instead of distinguishing it into elastic, visco-elastic, plastic and creep (linear and nonlinear) deformation to convert respectively.

The revise energy method does not require the SL strain–time curve to be of equal duration for each stress load level. With examination, the revise energy method is at least feasible to convert the later stage strain–time curves of triaxial creep tests of clayey soil. Through primary research, at the later stages of loading, compared with the disparity of strain between the measured SL and measured RL, the disparity of strain between the converted RL and measured RL decreases by 52.5%~53.5%.

With the revise energy method, much closer results to the practical results of RL creep tests can be obtained by converting the SL results so that the researchers can still choose SL in the soil triaxial creep test with the advantages of SL. Based on the more reliable converted strain–time curves, more accurate creep constitutive models are expected to be developed, and accordingly, engineering activities will benefit from the guidance of analysis on more practical strain–time curves and better constitutive models.

Author Contributions: Conceptualization, H.Q.; methodology, H.Q.; Software, H.Q., D.M.; validation, H.Q.; formal analysis, H.Q.; investigation, Z.N.; resources, A.T.; data curation, H.Q.; writing—original draft preparation, H.Q.; writing—review and editing, H.Q., D.M., Z.N., A.T.; visualization, H.Q.; supervision, A.T.; project administration, A.T., H.Q.; funding acquisition, A.T. All authors have read and agreed to the published version of the manuscript.

Funding: This research was funded by [National Natural Science Foundation of China] grant number [41672287] and the APC was funded by [Harbin Institute of Technology]. The author Qu, H. was also funded by [China Scholarship Council] grant number [202106120229] during the preparation, submission and publication period of this research.

Data Availability Statement: The data presented in this study are available on request from the corresponding author. The data are not publicly available due to the original authors of the data didn't present the data directly in number but in illustration in the cited literature.

Conflicts of Interest: The authors declare no conflict of interest.

References

- Liingaard, M.; Augustesen, A.; Lade, P.V. Characterization of Models for Time-Dependent Behavior of Soils. *Int. J. Géoméch.* **2004**, *4*, 157–177. [[CrossRef](#)]
- Sun, J. *Rheology of Geotechnical Materials and Its Engineering Application*; China Construction Industry Press: Beijing, China, 1999.
- Zhai, Y.; Wang, Y.; Dong, Y. Modified Mesri Creep Modelling of Soft Clays in the Coastal Area of Tianjin (China). *Teh. Vjesn.-Tech. Gaz.* **2017**, *24*, 1113–1121. [[CrossRef](#)]
- Jiang, Y.Z.; Wang, R.H.; Zhu, J.B. Rheological mechanical properties of altered-rock. *Mater. Res. Innov.* **2015**, *19*, S5-349–S5-355. [[CrossRef](#)]
- Ou, Z.-F.; Fang, Y.-G. The Influence of Organic Matter Content on the Rheological Model Parameters of Soft Clay. *Soil Mech. Found. Eng.* **2017**, *54*, 283–288. [[CrossRef](#)]
- Han, B.; Fu, Q. Study on the Estimation of Rock Rheological Parameters under Multi-level Loading and Unloading Conditions. *MATEC Web Conf.* **2018**, *213*, 02003. [[CrossRef](#)]
- Li, K.-F.; Liu, R.; Qiu, C.-L.; Tan, R.-J. *Consolidated Drained Creep Model of Soft Clay in Tianjin Coastal Areas*; Springer: Singapore, 2018; pp. 157–165. [[CrossRef](#)]
- Wang, Z.; Wong, R.C.K. Strain-Dependent and Stress-Dependent Creep Model for a Till Subject to Triaxial Compression. *Int. J. Géoméch.* **2016**, *16*, 04015084. [[CrossRef](#)]

9. Li, J.; Tang, Y.; Feng, W. Creep behavior of soft clay subjected to artificial freeze–thaw from multiple-scale perspectives. *Acta Geotech.* **2020**, *15*, 2849–2864. [[CrossRef](#)]
10. Hu, K.; Shao, J.-F.; Zhu, Q.-Z.; Zhao, L.-Y.; Wang, W.; Wang, R.-B. A micro-mechanics-based elastoplastic friction-damage model for brittle rocks and its application in deformation analysis of the left bank slope of Jinping I hydropower station. *Acta Geotech.* **2020**, *15*, 3443–3460. [[CrossRef](#)]
11. Zhang, G.; Chen, C.; Zornberg, J.G.; Morsy, A.M.; Mao, F. Interface creep behavior of grouted anchors in clayey soils: Effect of soil moisture condition. *Acta Geotech.* **2020**, *15*, 2159–2177. [[CrossRef](#)]
12. Yao, X.; Qi, J.; Zhang, J.; Yu, F. A one-dimensional creep model for frozen soils taking temperature as an independent variable. *Soils Found.* **2018**, *58*, 627–640. [[CrossRef](#)]
13. Bhat, D.; Kozubal, J.; Tankiewicz, M. Extended Residual-State Creep Test and Its Application for Landslide Stability Assessment. *Materials* **2021**, *14*, 1968. [[CrossRef](#)]
14. Liu, Z.B.; Xie, S.Y.; Shao, J.F.; Conil, N. Multi-step triaxial compressive creep behaviour and induced gas permeability change of clay-rich rock. *Géotechnique* **2018**, *68*, 281–289. [[CrossRef](#)]
15. Zhang, Y.Q. Research on Creep Model Test of Rockfill Material. Master’s Thesis, China Academy of Water Resources and Hydropower Sciences, Beijing, China, June 2013.
16. Shen, Z.J.; Zuo, Y.M. Experimental research on rheological properties of rockfill. In Proceedings of the 6th Symposium on Soil Mechanics and Foundation Engineering of the Chinese Society of Civil Engineering, Shanghai, China, 18–22 June 1991; pp. 443–446.
17. Cheng, Z.L.; Ding, H.S. Creep test for rockfill. *Chin. J. Geotech. Eng.* **2004**, *26*, 473–476.
18. Zhao, L.; Gan, H.X.; Tang, W.; Tang, M.F.; Zhou, H.P. Applicability Analysis of Chen’s Method in the Research of TATB-based PBX Creep Behavior. *Chin. J. Energetic Mater.* **2018**, *26*, 608–613. [[CrossRef](#)]
19. Zhao, X.; Wang, Q.; Gao, Y.; Yang, T.; He, L.; Lu, X. Indoor Rheological Test and Creep Model Analysis of Soft Soil in Qingyi River region in Wuhu Anhui. *IOP Conf. Series: Earth Environ. Sci.* **2019**, *330*, 032007. [[CrossRef](#)]
20. Tan, T.K.; Kang, W.F. Locked in stresses, creep and dilatancy of rocks, and constitutive equations. *Rock Mech.* **1980**, *13*, 5–22. [[CrossRef](#)]
21. Zhao, D.; Gao, Q.-F.; Hattab, M.; Hicher, P.-Y.; Yin, Z.-Y. Microstructural evolution of remolded clay related to creep. *Transp. Geotech.* **2020**, *24*, 100367. [[CrossRef](#)]
22. Nie, Z. Experimental Investigation on the Long-Term Properties of Expansive Soils Subjected to Freeze-Thaw Cycling. Master’s Thesis, Harbin Institute of Technology, Harbin, China, June 2018.
23. Tan, T.K. Basic Nature and Engineering Suggestions of Loess in Northwest China. *Chin. J. Geotech. Eng.* **1989**, *4*, 9–24.
24. Sun, J. Rock rheological mechanics and its advance in engineering applications. *Chin. J. Rock Mech. Eng.* **2007**, *26*, 1081–1106.
25. Zhang, X.W.; Wang, C.M.; Zhang, S.H. Comparative analysis of soft clay creep data processing method. *J. Jilin Univ. (Earth Sci. Ed.)* **2010**, *40*, 1401–1408. [[CrossRef](#)]
26. Kishi, M.; Tani, K. Development of measuring method for axial and lateral strain distribution using CCD sensor in triaxial test. In *Deformation Characteristics of Geomaterials*; IS: Lyon, France, 2003; pp. 31–36. [[CrossRef](#)]
27. Chu, J.; Lo, S.R.; Lee, I.K. Instability of Granular Soils under Strain Path Testing. *J. Geotech. Eng.* **1993**, *119*, 874–892. [[CrossRef](#)]
28. Li, S.; Huang, X.; Wu, S.; Tian, J.; Zhang, W. Bearing capacity of stabilized soil with expansive component confined by polyvinyl chloride pipe. *Constr. Build. Mater.* **2018**, *175*, 307–320. [[CrossRef](#)]
29. Zhou, P.J. Study on Shear Creep Characteristics and Model of Saturated Cohesive Soil. Master’s Thesis, Zhejiang University of Technology, Hangzhou, China, June 2018.